Thin Solid Films 520 (2012) 3433–3439

Contents lists available at SciVerse ScienceDirect

Thin Solid Films

journal homepage: www.elsevier.com/locate/tsf

Phase transformations in sputtered Ni–Mn–Ga magnetic shape memory alloy thin films

N. Jetta [a], N. Ozdemir [b], S. Rios [b], D. Bufford [b], I. Karaman [a,b], X. Zhang [a,b,*]

[a] Dept. of Mechanical Engineering, Texas A&M University, College Station, TX 77843-3123, USA
[b] Materials Science and Engineering Program, Texas A&M University, College Station TX 77842-3003, USA

ARTICLE INFO

Article history:
Received 10 December 2010
Received in revised form 4 December 2011
Accepted 11 December 2011
Available online 16 December 2011

Keywords:
NiMnGa
Magnetic shape memory alloys
Phase segregation
In situ x-ray diffraction

ABSTRACT

Ni–Mn–Ga magnetic shape memory alloy films have been prepared by the DC magnetron sputtering technique. As-deposited films show a quasi-amorphous structure that crystallizes at ~500 K. Crystallization study using Kissinger's analysis reveals a relatively low activation energy indicating partial crystallinity in the films. In situ X-ray diffraction studies show reversible martensite phase transformations, and phase segregation to non-transforming $L1_2$ precipitates at higher temperatures. It was observed that the phase segregation can be suppressed by low temperature heat treatment.

1. Introduction

There has been continuous technological interest and challenge in developing active actuator materials that exhibit large strains with a rapid response [1]. A number of active materials like rare earth alloys, $TbFe_2$, Terfenol-D that show magnetostriction of a few tenths of a percent strain under an applied magnetic field [2,3] have been proposed as magnetic actuator materials. These alloys are plagued with some disadvantages like poor electrical and thermal conductivity at elevated frequencies (unless they are used with small lateral dimensions). On the other hand shape memory alloys that undergo a diffusionless, displacive, martensitic transformation can exhibit super-elasticity and much greater thermally recoverable strains [4–9], but the temperature induced martensitic phase transformation has a very low response frequency. For practical field-induced-strain type of applications such as actuators, larger actuation strains at high operation frequencies are desirable, and magnetic shape memory alloys (MSMAs) have recently become promising candidates [10–14]. In Heusler alloys with Mn, the indirect exchange interaction between magnetic ions results in ferromagnetism [14]. Hence in MSMAs, the magnetic field can change martensitic phase transformation temperatures, and correspondingly tailor the shape and dimensions of MSMAs, a so called magnetic shape memory effect.

MSMAs exhibit strong interactions between their crystal structures and magnetic properties. In MSMAs such as Ni–Mn–Ga alloys where the difference in the Zeeman energy of existing phases is low, the difference in the magneto-crystalline anisotropy energy of the martensite variants is harnessed to demonstrate magnetic field induced re-orientation (MFIR) [15]. Ni_2MnGa system, which belongs to the family of Heusler alloys, has received significant attention after it was observed that ~0.2% of strain can be induced by magnetic field of 6.366×10^5 A/m at 265 K [10]. Since then considerable progress has been made in understanding the MFIR effect in bulk Ni–Mn–Ga alloys.

In comparison to their bulk counterparts, Ni–Mn–Ga thin films have also received significant attention due to their applications as actuators and scanners [16–23]. Compared to their bulk counterparts, Ni–Mn–Ga thin films may have better mechanical strength and ductility [24,25] and unique magnetic properties [26–34]. For thin films, control of composition, microstructure, such as precipitation is more challenging. Several physical properties of Heusler alloys that dictate the magnetic shape memory effect are very sensitive to composition [2,35]. Chernenko et al. correlated physical properties, such as phase transformation temperature, to valence electron concentration per atom (e/a) [36]. Such correlation reveals that a 0.1 unit change in e/a can lead to the variation of martensite start temperature (M_s) by as large as 70 K in Ni–Mn–Ga system [36].

Magnetron sputtering and pulsed laser deposition techniques are frequently used to deposit films of these systems [37–43]. Sputtering deposition parameters, such as deposition rate and substrate bias, have influence on the composition of films [44,45]. Ni–Mn–Ga films deposited at room temperature are known to be partially crystalline with little or no magnetic and shape memory properties [31,43,46–50]. Microstructures and phase transformations in these systems have also been investigated [51–61], where both 10 M and 14 M martensites have been observed [62,63]. Size effects have also been identified

* Corresponding author at: Dept. of Mechanical Engineering, Texas A&M University, College Station, TX 77843-3123, USA. Tel.: +1 979 845 2143.
E-mail address: zhangx@tamu.edu (X. Zhang).

0040-6090/$ – see front matter © 2011 Elsevier B.V. All rights reserved.
doi:10.1016/j.tsf.2011.12.029

where the phase transformation behaviors depend on film thickness [64–70]. In addition, grain boundaries in polycrystalline MSMAs act as barriers for magnetic field induced shape change, while structural ordering is necessary for the magnetic dipoles in the unit cells to align under magnetic field [48]. Hence annealing is necessary for structural ordering and grain growth in thin films that facilitates ferromagnetic and shape memory behavior. In bulk Ni–Mn–Ga alloys it was observed that thermal annealing caused precipitation of γ phase with disordered A1 structure, which later transforms to γ′ phase [71]. Furthermore γ′ precipitate has $L1_2$ crystal structure and is a non-transforming phase (γ precipitates also appear non-transformable) and hence degrade shape memory performance. Precipitation of non-transformable phases poses a serious problem by introducing localized stresses and composition inhomogeneity. The precipitation issue is more pronounced in thin films due to their large surface area. The greater surface energy in the films may drive system further away from the equilibrium energy state, and hence provides greater driving force to precipitation processes in films in comparison to bulk counterparts.

In order to develop MEMS devices using Ni–Mn–Ga films for future actuators, it is important to understand the precipitation and phase transformation characteristics in these thin films subjected to heat treatment. In this paper, we report the synthesis and microstructure of Ni-rich Ni–Mn–Ga free-standing thin films, and a systematic study of phase transformation and precipitation in these films.

2. Experimental methods

Ni–Mn–Ga thin films, ~5 μm in thickness, were fabricated using DC magnetron sputtering technique from a $Ni_{49.5}Mn_{30.3}Ga_{20.2}$ target on unheated SiO_2 substrate. Prior to deposition a base pressure of $<1.2\times10^{-5}$ Pa is typically achieved. The deposition was then carried out at an Ar pressure of $\sim3.3\times10^{-1}$ Pa. Free-standing films were obtained by peeling off the thick films from substrates without introducing significant mechanical damage into the films. The composition of the films was determined by wavelength dispersive spectroscopy (WDS) technique using a *Cameca SX40 electron microprobe* with approximately 1 at.% accuracy. Crystal structure and phases of films were examined using *Bruker AXS D8 Advanced Bragg Brentano X-ray Diffractometer* with Cu–K_α radiation. Transmission electron microscopy (TEM) experiments were performed on a *JEOL JEM-2010* transmission electron microscope operated at 200 kV. Indentation modulus and hardness were obtained using instrumented nanoindentation technique with a *Fisherscope HM2000 XYp* micro/nanoindentor. Indentation depth was kept to less than 10% of total film thickness and 9–12 indents were performed to obtain average value and standard deviations.

The phase transformations of as-deposited free-standing films have been studied using differential scanning calorimetry (DSC) technique on a *TA instruments Q1000* differential scanning calorimeter. Phase transformation has also been studied in situ using a *Bruker AXS D8 X-ray diffractometer* with a Beryllium-dome temperature stage (MRI, BTS-Basic). The high temperature stage covered with hemispherical Beryllium dome is connected to mechanical and turbo molecular pump attachments for achieving high vacuum ($\sim1\times10^{-4}$ Pa). The alumina sample stage uses a Pt (Platinum) heating strip to achieve temperatures as high as 1500 K. A water-cooling system attached to the dome enables stable temperature controls. The heating (cooling) rate during the in situ X-ray diffraction (XRD) experiments was 10 K/min. Grain growth and phase transformations were also examined by in situ TEM experiments. The measured temperature during in situ XRD and TEM experiments is calibrated to be within ±5 and 10 K of preset values, respectively. Powdercell [72] and Checkcell [73] software are used to determine crystal structures. A *Quantum Design MPMS SQUID VSM* has been used to measure magnetic properties of thin films both in-plane and out-of-plane. Magnetization vs. temperature curves were obtained by first cooling the specimens under zero field, and then applying a certain magnetic field during heating process.

3. Results

The composition of the sputtered films determined by WDS is $Ni_{53}Mn_{29}Ga_{18}$. XRD pattern of as-deposited films shown in Fig. 1 reveals a single broad peak with peak position at 43.1°, indicating a combination of amorphous and nanocrystalline nature of the films. The average grain size analyzed by using the Scherrer's equation [74] and measured full width half maximum (FWHM) is ~7 nm. To study the mechanical properties, thin films (~5 μm in thickness) on SiO_2 substrate were indented at a depth of 100–400 nm using nanoindentation. A plateau of hardness vs. indentation depth is observed. An example is shown in Fig. 2. The indentation hardness is measured to be 7.0 ± 0.2 GPa, and the indentation modulus is 133 ± 7 GPa.

As-deposited free standing films were subjected to controlled heating and cooling at different rates in DSC. In the first heating cycle, an exothermic peak corresponding to the crystallization of amorphous structure is observed as shown in Fig. 3. Subsequent cooling and heating lead to a reversible austenite (A) to martensite (M) phase transformation as shown by segments 2 and 3 in Fig. 3. Fig. 4a shows isochronous heating curves for the as-deposited films tested at heating rates of 10, 20 and 40 K/min. The crystallization temperatures, varying from ~493 to 523 K at different heating rates, were used to calculate the activation energy for crystallization using the Kissinger's equation [75]:

$$\ln\left(\frac{\beta}{T_p^2}\right) = C - \frac{E_a}{RT_p} \tag{1}$$

where, T_p is the peak crystallization temperature, β is the heating rate, E_a is the effective activation energy for crystallization, R is the gas constant, C is a constant. The activation energy E_a is calculated to be 157 ± 13 kJ/mol as shown in Fig. 4b.

Numerous heating and cooling cycles were performed on a 5 μm thick, free-standing film during in situ XRD experiments to study phase transformations. Magnified XRD results are presented for the first heating cycle in Fig. 5a, at 423 K or lower, a broad peak is observed at ~43°. At 523 K, crystallization is evident, and the major peak is identified as $L2_1$ (022) (Fm3m; a = 5.84 Å), and the small left-shoulder peak is determined to be $L1_2$ (111) (Pm3m; a = 3.689 Å). On further heating the intensity of $L2_1$ (022) peak diminishes sharply, meanwhile the $L1_2$ (111) peak becomes predominant. During the second heat-cool cycle, as shown in Fig. 5b, the diminished $L2_1$ (022) peak is still discernable manifested as a small right shoulder peak. Complete XRD patterns during the second heat-cool cycle are shown in Fig. 5c. Several features are noteworthy. First, a majority of XRD peaks appear to originate from $L1_2$ phase that does not transform during heating and cooling experiments. Second, $L2_1$ phase, indicated by $L2_1$ (004) peak, at 2 theta of ~64° degree, clearly went through a reversible phase transformation at

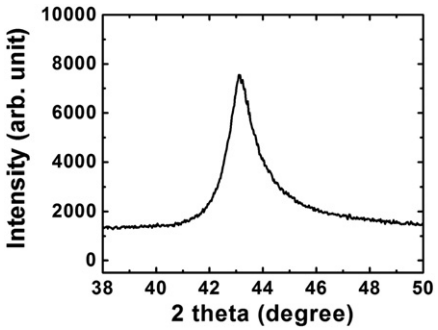

Fig. 1. XRD of as-deposited $Ni_{53}Mn_{29}Ga_{18}$ films on oxidized Si (100) substrate. A broad peak is observed at ~43.1°.